

UCLA

UCLA Previously Published Works

Title

Anthropogenic Intensification of Cool-Season Precipitation Is Not Yet Detectable Across the Western United States

Permalink

<https://escholarship.org/uc/item/2q81q3gg>

Journal

Journal of Geophysical Research: Atmospheres, 129(12)

ISSN

2169-897X

Authors

Williams, A Park
McKinnon, Karen A
Anchukaitis, Kevin J
et al.

Publication Date

2024-06-28

DOI

10.1029/2023jd040537

Peer reviewed










RESEARCH ARTICLE

10.1029/2023JD040537

Anthropogenic Intensification of Cool-Season Precipitation Is Not Yet Detectable Across the Western United States

Key Points:

- Over 1951–2023, precipitation on the wettest cool-season days did not increase across most of the western US, and even declined in areas
- In California, most climate models do not project human-caused precipitation intensification to become detectable before the 2060s
- Climate models rarely simulate precipitation intensity to decline as much as it did in northern California and the Pacific Northwest

A. Park Williams^{1,2,3} , Karen A. McKinnon^{2,4,5} , Kevin J. Anchukaitis^{3,6,7} , Alexander Gershunov⁸ , Arianna M. Varuolo-Clarke^{3,9} , Rachel E. S. Clemesha⁸ , and Haibo Liu³ 

¹Department of Geography, University of California, Los Angeles, Los Angeles, CA, USA, ²Department of Atmospheric and Oceanic Sciences, University of California, Los Angeles, Los Angeles, CA, USA, ³Lamont-Doherty Earth Observatory, Columbia University, Palisades, NY, USA, ⁴Department of Statistics and Data Science, University of California Los Angeles, Los Angeles, CA, USA, ⁵Institute of the Environment and Sustainability, University of California Los Angeles, Los Angeles, CA, USA, ⁶School of Geography, Development, and Environment, University of Arizona, Tucson, AZ, USA, ⁷Laboratory of Tree-Ring Research, University of Arizona, Tucson, AZ, USA, ⁸Scripps Institution of Oceanography, University of California, San Diego, CA, USA, ⁹Department of Earth and Environmental Sciences, Columbia University New York, New York, NY, USA

Supporting Information:

Supporting Information may be found in the online version of this article.

Correspondence to:

A. P. Williams,
williams@geog.ucla.edu

Citation:

Williams, A. P., McKinnon, K. A., Anchukaitis, K. J., Gershunov, A., Varuolo-Clarke, A. M., Clemesha, R. E. S., & Liu, H. (2024). Anthropogenic intensification of cool-season precipitation is not yet detectable across the Western United States. *Journal of Geophysical Research: Atmospheres*, 129, e2023JD040537. <https://doi.org/10.1029/2023JD040537>

Received 1 DEC 2023
Accepted 23 MAY 2024

Author Contributions:

Conceptualization: A. Park Williams, Karen A. McKinnon, Kevin J. Anchukaitis, Alexander Gershunov, Rachel E. S. Clemesha
Data curation: A. Park Williams, Karen A. McKinnon, Arianna M. Varuolo-Clarke, Haibo Liu
Formal analysis: A. Park Williams
Funding acquisition: A. Park Williams
Investigation: A. Park Williams
Methodology: A. Park Williams, Karen A. McKinnon, Kevin J. Anchukaitis, Alexander Gershunov
Project administration: A. Park Williams

Abstract The cool season (November–March) of 2022–2023 was exceptional in the western United States (US), with the highest precipitation totals in ≥ 128 years in some areas. Recent precipitation extremes and expectations based on thermodynamics motivate us to evaluate the evidence for an anthropogenic intensification of western US cool-season precipitation to date. Over cool seasons 1951–2023, trends in precipitation totals on the wettest cool-season days were neutral or negative across the western US, and significantly negative in northern California and parts of the Pacific Northwest, counter to the expected net intensification effect from anthropogenic forcing. Multiple reanalysis data sets indicate a corresponding lack of increase in moisture transports into the western US, suggesting that atmospheric circulation trends over the North Pacific have counteracted the increases in atmospheric moisture expected from warming alone. The lack of precipitation intensification to date is generally consistent with climate model simulations. A large ensemble of 648 simulations from 35 climate models suggests it is too soon to detect anthropogenic intensification of precipitation across much of the western US. In California, the 35-model median time of emergence for intensification of the wettest days is 2080 under a mid-level emissions scenario. On the other hand, observed reductions of precipitation extremes in California and the Pacific Northwest are near the lower edge of the large ensemble of simulated trends, calling into question model representation of western US precipitation variability.

Plain Language Summary After warming, one of the best understood climate responses to greenhouse gasses is increased atmospheric moisture (from more evaporation) and resultant storm intensification. Given that hydrological infrastructure and policies are probably more attuned to past climate than future climate, intensified precipitation has important implications for management of flood hazards and water resources. In the western US, the very wet winter of 2023 and the extensive flooding that resulted indicated that this region may be highly vulnerable to increases in precipitation extremes. Are precipitation extremes already intensifying in the western US? We find no evidence for intensified western US winter precipitation thus far. In fact, precipitation intensity actually decreased in northern California and the Pacific Northwest over 1951–2023. In California, most climate models do not project intensified precipitation to become detectable from that region's wide range of natural variability until the 2060s even under heavy greenhouse-gas emissions. By the end of this century, however, most climate models consistently project the strongest storms to be stronger than they were historically across most or all of the western US. Thus, the lack of precipitation intensification thus far should not dissuade planning for greater precipitation intensity and flood risks.

© 2024. The Author(s).

This is an open access article under the terms of the [Creative Commons Attribution License](https://creativecommons.org/licenses/by/4.0/), which permits use, distribution and reproduction in any medium, provided the original work is properly cited.

1. Introduction

The cool season of 2023 (November 2022–March 2023) was exceptionally wet in the western United States (US). Heavy storms accompanied by cool temperatures delivered large mountain snowpacks and drought relief across much of the region, while also causing widespread flooding and associated hydrological hazards. In winter and spring 2023, President Biden granted two Major Disaster Declarations in California following flooding and

Resources: A. Park Williams
Validation: A. Park Williams
Visualization: A. Park Williams
Writing – original draft:
 A. Park Williams
Writing – review & editing:
 A. Park Williams, Karen A. McKinnon,
 Kevin J. Anchukaitis,
 Alexander Gershunov, Arianna
 M. Varuolo-Clarke, Rachel
 E. S. Clemesha, Haibo Liu

landslides. High precipitation totals and low temperatures combined to produce a 237%-of-average Sierra Nevada April 1 snowpack (<https://cww.water.ca.gov/yearly-summary>), potentially the largest since at least 1952 (Marshall et al., 2024). Runoff from the southern Sierra Nevada subsequently caused the reflooding of the ancient Tulare Lake in California's southern Central Valley, which was drained for agriculture in the late 1800s and early 1900s. Were these extreme conditions in 2023 promoted by anthropogenic climate change?

As the atmosphere warms, its saturation vapor pressure rises exponentially and models project enhanced atmospheric moisture as a result, making more water available for precipitation during strong storms (Fischer et al., 2014; O’Gorman & Schneider, 2009; Pfahl et al., 2017; Trenberth, 1999). On the other hand, models project a slower global atmospheric circulation as well as atmospheric stabilization in some regions, increasing the frequency of days with little or no precipitation throughout much of the tropics and mid-latitudes (Giorgi et al., 2011; Polade et al., 2014; Sun et al., 2007). In the western US and many other regions globally, the net expected result is precipitation concentrated into fewer events and enhanced interannual volatility of precipitation totals (Gershunov et al., 2019; Pendergrass et al., 2017; Polade et al., 2017; Rind et al., 1989; Swain et al., 2018). Thus, there is theoretical underpinning for the interpretation that anthropogenic climate change may have promoted the very wet cool season of 2023, as well as those of 2017 and 2019, in the western US even as the region was otherwise in an extended drought, which was also intensified by anthropogenic forcing (Williams et al., 2022).

In fact, despite only a small simulated effect of anthropogenic climate change on mean annual precipitation totals, the previous version of the Community Earth System Large Ensemble (Kay et al., 2015) suggested that anthropogenic forcing from 1850 to 2022 approximately doubled the probability of a month as wet as the one that caused infamous statewide flooding in California in 1862 and temporarily turned its Central Valley into an inland sea (Huang & Swain, 2022). This result was based on just one climate model, however, and models vary greatly in terms of how regional precipitation intensity responds to anthropogenic forcing (Norris et al., 2021; O’Gorman, 2015; Pierce et al., 2023).

A major source of uncertainty regarding anthropogenic impacts on precipitation extremes is aerosols (Hegerl et al., 2015; Pendergrass & Hartmann, 2012; Risser et al., 2023, 2024; Samset et al., 2016). In general, models simulate a weak negative forcing from anthropogenic aerosols on global precipitation extremes over the historical period because aerosol shading reduces evaporation and atmospheric moisture content (Baek & Lora, 2021; Dong et al., 2021; Liepert et al., 2004; Ramanathan et al., 2001; Wu et al., 2013). However, aerosols are simulated to have a multitude of other effects on precipitation as well, including via effects on cloud properties and atmospheric circulation, that play out across a range of timescales and are highly variable geographically, seasonally, and by aerosol type (Myhre et al., 2017; Risser et al., 2023; Samset et al., 2016; Tao et al., 2012). In the US, Risser et al. (2024) estimated that anthropogenic aerosols have masked a substantial portion of the precipitation intensification that would have otherwise been expected from greenhouse-gas forcing alone. However, this net effect averaged over the continental US appears strongest in summer and fall, when the western US is relatively dry. In addition, the detection and attribution approach developed by Risser et al. (2023, 2024) suggests the aerosol effect on western US precipitation extremes has thus far been dominated by the atmosphere’s “fast” responses to energy-balance changes. On the other hand, Risser et al. (2024) also show that idealized-model simulations (Myhre et al., 2017) suggest the western US aerosol effect is dominated by “slow” responses to surface cooling. Overall, anthropogenic aerosols likely impact precipitation extremes in the western US and beyond but their effects are complex and uncertain.

Another major source of uncertainty regarding anthropogenic effects on precipitation extremes arises from the forced response of atmospheric circulation, as opposed to the forced thermodynamic response of atmospheric humidity, especially in the mid-latitudes (Norris et al., 2019; Pfahl et al., 2017). In the western US, projections of circulation-driven changes in precipitation extremes tend to be negative in the south due to enhanced subtropical subsidence and positive in the north, but with much variability among individual models (Huang & Stevenson, 2021; Pfahl et al., 2017). Combined, the net modeled response of thermodynamics and atmospheric circulation to anthropogenic forcing is increased precipitation on the wettest cool-season days across the western US, but with high spatial heterogeneity and uncertainty in the magnitudes of these trends.

Although warming-driven increases in precipitation intensity have already been identified at the global and hemispheric scales (Allan & Soden, 2008; Min et al., 2011; O’Gorman & Schneider, 2009; Sun et al., 2021), they have not been observed across much of the western US, and numerous studies have shown apparent reductions in

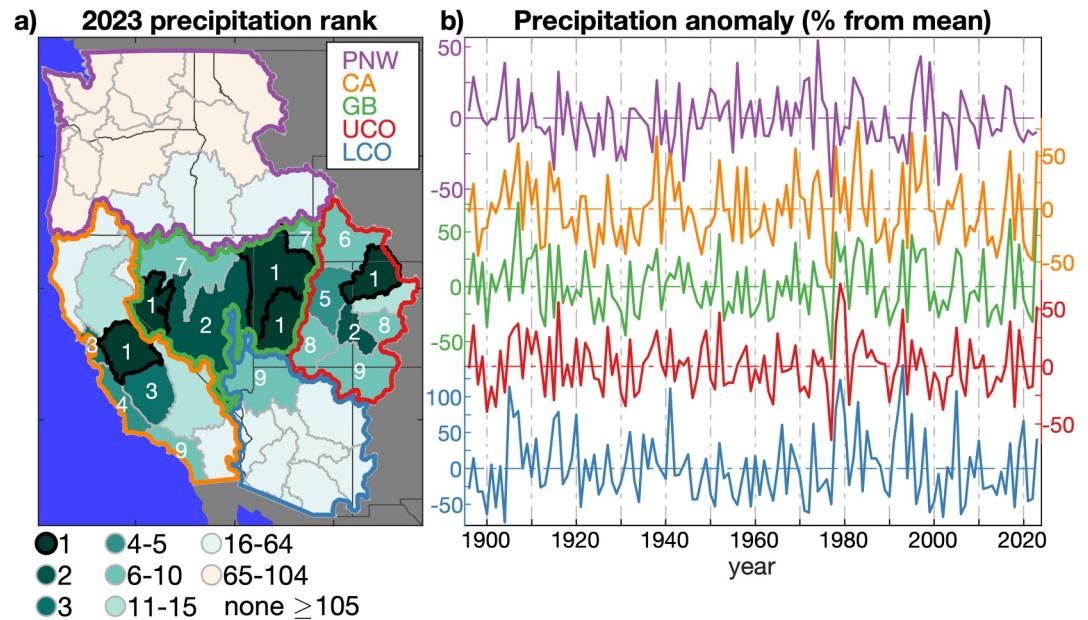


Figure 1. 2023 cool-season (November–March) precipitation anomalies in a 128-year context. (a) Ranking of the 2023 cool-season precipitation total among cool seasons 1896–2023 according to monthly nClimGrid for each of 44 western US HUC-4 hydrological regions. Ranking of one indicates cool-season 2023 was wettest on record. Top-10 rankings are printed in white. Thick colored polygons bound the larger HUC-2 regions (PNW: Pacific Northwest, CA: California, GB: Great Basin, UCO: Upper Colorado River, LCO: Lower Colorado River). (b) Time series of cool-season precipitation anomalies for each of the 5 HUC-2 regions (colors correspond to the regions as defined in the legend in (a)). Anomalies are percent deviations from the 1951–2023 mean.

precipitation intensity along the Pacific coast (Gershunov et al., 2019; Harp & Horton, 2022; Kunkel et al., 2020; Luce et al., 2013; Sun et al., 2021). Given an apparent lack of observed intensification in the western US, is there a case for anthropogenic forcing as a driver of the high precipitation totals in cool-season 2023? If not, why? When should the projected anthropogenic intensification of cool-season precipitation become detectable in the western US? And where should this signal first appear?

Here we address the above questions with a comprehensive analysis of observed and modeled daily precipitation in the western US as well as global reanalyses of historical atmospheric circulation. First, we use uniquely long and continuous gauge records to assess trends in cool-season precipitation frequency and intensity, including precipitation totals on the wettest days, across the western US since 1951 and we evaluate anomalies in 2023 in the context of the longer-term trends. Second, we analyze moisture transports into regions of the western US on their wettest cool-season days to understand the importance of atmospheric moisture content and circulation to western US extreme precipitation as well as how and why moisture transports have changed since 1951. Third, we evaluate 648 simulations of daily precipitation from 35 state-of-the-art climate models to assess the degree to which observed trends in western US cool-season precipitation intensity are consistent with model-based expectations. We conclude by determining when climate models project anthropogenic intensification of cool-season precipitation to emerge as distinguishable from natural variability and how the timing of this emergence varies geographically across the western US.

2. Materials and Methods

2.1. Study Region and Season

Our study area is the western US, which we treat as the 44 hydrological subregions west of the continental divide in the contiguous US as identified by the USGS 4-digit hydrological unit code (HUC-4) (gray boundaries in Figure 1a). Each subregion sits in one of five larger HUC-2 regions bounded by bold colors in Figure 1a (Pacific Northwest, California, Great Basin, Upper Colorado, Lower Colorado).

We focus on the cool season of November–March because of the disproportionate contribution of intense precipitation in these months to water resources and flood hazards, particularly in California (Dettinger, 2016). Maps of mean cool-season precipitation totals and relative contributions to water-year precipitation totals are provided in Figures S1a and S1b in Supporting Information S1.

2.2. Daily Gridded Precipitation Totals for Cool Seasons 1951–2023

We produce daily fields of gridded precipitation totals for cool seasons 1951–2023 at 0.25° geographic resolution based on 642 gauges from the Global Historical Climatology Network (GHCN)-Daily (Menne, Durre, Vose, et al., 2012). Because our study is about trends, we only use gauges with observations for $\geq 75\%$ of cool-season days in each of the 8 decades of our study period (1951–1960, . . . , 2011–2020, 2021–2023). After gauge selection, we fill daily gaps using nearby gauges and quantile mapping. We detail the methods to create this data set in Text S1 in Supporting Information S1. A map of gauge locations is provided in Figure S2 in Supporting Information S1. Figure S2 in Supporting Information S1 also shows gauge-level trends in cool-season precipitation total, frequency, and intensity (defined in Section 2.4) and demonstrates that the general geographic patterns of trends among the 642 gauges are also present among trends calculated from raw data at a subset of 321 gauges with especially continuous records ($\geq 90\%$ of daily data for $\geq 90\%$ of 1951–2023 cool seasons). Our regional records of cool-season precipitation totals correlate strongly ($r \geq 0.98$) with those calculated from the National Atmospheric and Oceanic Administration (NOAA) monthly nClimGrid (Vose et al., 2014) and PRISM (Daly et al., 2008), promoting confidence in the accuracy of our data set (Figure S3 in Supporting Information S1).

We produce our own gridded daily precipitation data set because, to our knowledge, the only other gridded daily gauge-based precipitation data sets extending back to the mid-20th century for the western US, the daily nClimGrid data set covering 1951–present (Durre, Arguez, et al., 2022) and the data set from the NOAA Climate Prediction Center (CPC) covering 1948–present, do not include long and continuous data coverage as a necessary criterion for gauge inclusion. Results based on these data sets could thus be interpreted as sensitive to the large regional changes in gauge density that occurred across the western US since the mid-20th century (Figure S4 in Supporting Information S1). This interpretation is supported Durre, Arguez, et al. (2022) in their introduction of the daily nClimGrid data set. In their assessment of trends in extreme precipitation, they confined their analysis to 1981–2015 due to the widespread distribution of gauges with relatively complete records during that period. See Text S2 and Figures S5–S10 in Supporting Information S1 for a comparison of our GHCN data set to the nClimGrid and CPC products as well as the shorter 1981–present daily data set from PRISM (Daly et al., 2021) and an alternative version of our data set produced with a larger gauge network selected using more liberal inclusion criteria. Throughout the paper, we provide supplementary analyses comparing key results derived from our GHCN data set to those derived from daily nClimGrid. We do not consider the CPC data set due to curious trends in precipitation frequency (Figures S6 and S7 in Supporting Information S1) and lack of methods documentation.

2.3. Large-Scale Atmospheric Data

Our primary analyses of large-scale atmospheric conditions over the North Pacific and western North America are based on the ERA5 reanalysis from the European Center for Medium-Range Weather Forecasts, which covers 1940–present (Hersbach et al., 2020). We use this data set because it overlaps temporally with our daily precipitation data set and its relatively high spatial resolution has been found previously to better represent fine-scale vapor-transport features over coastal land (Marquardt Collow et al., 2022). We calculate integrated vapor transports (qv ; $\text{kg m}^{-1} \text{s}^{-1}$) from the surface to 300 hPa from 6-hourly grids of zonal and meridional wind velocity and specific humidity at 1° geographic resolution over the geographic domain 20–60°N, 160–100°W (we calculate near-surface specific humidity from 2-m temperature, relative humidity (RH), and surface pressure). For each time step and grid cell we calculate qv by taking the product of specific humidity (q ; kg/kg) and the wind velocity vector (v ; m/s) at the near-surface and each of the 20 available pressure levels from 1000 to 300 hPa (masking pressure levels below the surface), linearly interpolating at pressure steps of 1 hPa, averaging, multiplying by the pressure difference (in Pa) between the surface and 300 hPa, and dividing by gravitational acceleration. To visualize anomalies in the horizontal circulation of qv we also calculate its zonal and meridional components by replacing v with only the zonal or meridional component of wind velocity, respectively. We evaluate contributions from v variability to qv ($\bar{q}v$) by following the above method and, at each time step and pressure level, allowing v to vary while holding q at its 1951–2022 monthly climatology. We correspondingly

evaluate contributions from q ($q\bar{v}$) by allowing q to vary while holding v at its monthly climatology. For comparison we also consider the lower-resolution (2.5° , 8 pressure levels) reanalysis from the National Center for Environmental Protection and the National Center for Atmospheric Research (NCEP/NCAR) (Kalnay et al., 1996). For analyses of trends in large-scale atmospheric variables, we spatially aggregate ERA5 data to 2.5° -resolution to reduce the number of trend tests performed as well as to aid visualization of trend significance and comparison to NCEP/NCAR trends.

2.4. Precipitation Metrics

For each 0.25° grid cell in our daily precipitation data set we calculate cool-season precipitation total, wet-day frequency (number of days with precipitation ≥ 2 mm), and wet-day intensity (mean precipitation total on wet days), as well as a number of intensity metrics representing contributions from the wettest days, described below. We focus on wet days with ≥ 2 mm precipitation to avoid results being dominated by days with very low precipitation totals and because we found disagreement among daily precipitation data sets in terms of frequency of days with < 2 mm precipitation (Text S2 in Supporting Information S1). Daily values for each HUC-4 subregion and HUC-2 region are calculated as area-weighted means of the 0.25° gridded values within.

To assess precipitation extremes, we evaluate four commonly used metrics (Peterson & Manton, 2008; Zhang et al., 2011), described at <https://www.climdex.org/learn/indices/>. First, we evaluate the cool-season precipitation total from days when precipitation total exceeded the 95th percentile of all 1951–2023 cool-season wet-day totals ($R95p$) as well as each cool-season's largest single daily precipitation total ($Rx1day$). Traditionally $R95p$ is calculated from all days with ≥ 1 mm precipitation but we use our 2 mm wet-day threshold instead. We also evaluate the fractional contribution of $R95p$ and $Rx1day$ to each cool-season's total precipitation ($R95pTOT$ and $Rx1dayTOT$, respectively). For a supplementary analysis we evaluate each cool season's 3 (not necessarily consecutive) highest daily precipitation totals. See Figures S1c–S1f in Supporting Information S1 for maps of $R95p$, $Rx1day$, and their relative contributions to total cool-season precipitation.

2.5. Climate Model Data

Among climate models participating in the 6th phase of the Coupled Model Intercomparison Project (CMIP6) (Eyring et al., 2016), 35 made daily precipitation available for ≥ 1 continuous realization extending across the Historical (1850–2014) and future period (2015–2100) under the SSP2-4.5, which represents a mid-range future emissions scenario (O'Neill et al., 2016). We also consider realizations from the same 35 models under the higher-emissions SSP5-8.5 scenario in some analyses. For both scenarios, we use all available continuous realizations of Historical–SSP2-4.5 and Historical–SSP5-8.5 ($N = 294$ and 254 , respectively). We additionally consider the very large ensemble (100 realizations) of historical–SSP3-7.0 from the version-2 Community Earth System Model (Danabasoglu et al., 2020; Rodgers et al., 2021) to assess the role of internal variability in driving precipitation intensity trends. Table S1 in Supporting Information S1 lists the 35 models, their geographic resolutions, and the number of realizations considered for each scenario. For each realization we calculate a time series of daily precipitation for each HUC-4 subregion as the area-weighted mean total among overlapping model grid cells. We calculate the various annual metrics of cool-season precipitation intensity (e.g., $R95p$) from these subregional records and then calculate area-weighted averages of these subregional records for each HUC-2 region.

2.6. Statistical Analysis

We assess all trends using the Theil-Sen estimator, as this non-parametric estimator is less sensitive than least-squares regression to extreme values (Sen, 1968). To aid comparison of trends among regions and variables, we convert all HUC-4 subregional and HUC-2 regional time series to percent of the 1951–2023 mean. We assess each trend's significance with 5,000 block-bootstrapped replications where each time series' block length is determined from 1st-order autocorrelation following Wilks (1997) and each trend's p-value is estimated as the fraction of bootstrapped trend values that exceeded the observed trend in terms of absolute value (2-sided significance test). We also use the block bootstrap to evaluate significance of correlations.

For the CMIP6 time-of-emergence (TOE) analysis, we assess TOE for each continuous Historical–SSP2-4.5 realization of cool-season $R95p$ for each HUC-2 region, calculate the median TOE year among realizations from each model, and then calculate the multi-model median and interquartile TOE years. In supplementary analyses

we repeat the TOE assessment for $R95pTOT$, $Rx1day$, and $Rx1dayTOT$ as well as for $R95p$ under the SSP5-8.5 scenario. For each analysis and model realization, we consider the distribution of values during 1851–1950 to represent the historical baseline that we seek to detect TOE from. Although this period was not free of anthropogenic greenhouse-gas forcing, the forcing was weak compared to more recent decades and emergence of hydrological extremes from a 1851 to 1950 baseline is likely to be more societally relevant than emergence from a pre-industrial baseline. To test for emergence from baseline, for each realization we perform a Kolmogorov-Smirnov (KS) test on a rolling 21-year basis (1-year time step) from 1851 to 2100 to evaluate for significant ($p < 0.1$) differences from the baseline distribution. Our use of the KS test is consistent with methods used in other efforts to detect TOE in climate extremes (King et al., 2015; Mahlstein et al., 2012). Our choice of a 21-year moving window is in line with the 2-decade period used by King et al. (2015) to assess TOE in projected climate extremes.

A common approach is to declare TOE when significance is achieved only if no subsequent dips below the significance threshold (Lehner et al., 2017; Mahlstein et al., 2012). Here we employ a more liberal criterion to reduce the capacity for brief excursions below the significance threshold to prevent detection of an otherwise persistent signal. Once a sequence of significant deviations from baseline begins, we necessitate that $\geq 80\%$ rather than 100% of subsequent overlapping 21-year periods satisfy the significance test. If significance is achieved in a given 21-year window and remains for $\geq 80\%$ of subsequent windows (ending in 2080–2100), we consider the central year of the 1st period of emergence to be the TOE year, consistent with Lehner et al. (2017). Given our method, some detections of TOE late in the 21st century are likely premature due to limited subsequent opportunities for 21-year rolling distributions of $R95p$ to become indistinguishable from baseline (Hawkins et al., 2014). For example, a TOE of 2090 only indicates significant differences from baseline in the final overlapping 21-year window of the analysis period.

Finally, for all assessments of significance we use a relatively liberal threshold ($p < 0.1$) to assure that our finding of a general lack of extreme precipitation intensification is not due to a high standard for significance. However, repetition of many significance tests (e.g., a trend test for each of multiple regions) is likely to lead to findings of significance by random chance. In each analysis involving a significance assessment for multiple HUC-2 regions, HUC-4 subregions, or reanalysis grid cells, we adjust significance classifications for the expected false discovery rate (FDR) associated with the number of regional tests following Wilks (2016). Briefly, when multiple p -values are calculated (e.g., for each of 44 subregions) in a given analysis, all p -values are ranked in ascending order and compared to a corresponding vector of values ascending from α_{FDR}/N to α_{FDR} in steps of α_{FDR}/N , where α_{FDR} is the significance level used in the FDR test and N is the number of significance tests (e.g., 44). The upper-limit for significant p -values (p_{FDR}^*) is then defined as the largest p -value to be less than or equal to the corresponding vector ascending from α_{FDR}/N to α_{FDR} . Wilks recommends that for climate analyses where time series are moderately or highly spatially correlated (as is the case in our study), α_{FDR} should be $2\alpha_{global}$, where α_{global} is 0.1 in this study (thus, $\alpha_{FDR} = 2\alpha_{global} = 0.2$). If any p -value is $< p_{FDR}^*$ and also < 0.1 , then that and all lower p -values are assessed as statistically significant. Instances when $p < 0.1$ but not $< p_{FDR}^*$ are referred to as “marginally significant.” Significance reclassifications to account for FDR are repeated for each figure panel independently. In tests of simulated trends or distribution changes from CMIP6 models, FDR adjustments are made for each model realization independently to allow for direct comparison to observations.

3. Results

We first evaluate cool-season 2023 precipitation totals in the long-term context of 1896–2023 using the monthly NOAA nClimGrid data set (Vose et al., 2014). This initial analysis of long-term variations in seasonal totals back to the late 20th century uses the monthly NOAA nClimGrid data set instead of our daily product because this analysis does not require daily data and extends prior to 1951, the first year of our daily data set. According to monthly nClimGrid, cool-season 2023 ranks as wettest on record in 5 of 44 HUC-4 subregions, accounting for 11% of the western US area, and ranks among the wettest 10 cool seasons on record in 19 subregions (40% of western US) (Figure 1a). The largest anomalies in 2023 span from the central coast of California through Great Basin and Upper Colorado. Anomalies exceed +50% (relative to a 1951–2023 baseline) in California, Great Basin, and Upper Colorado but are not record-breaking in the 1896–2023 context for any HUC-2 region. Notably, no time series of regional or subregional cool-season precipitation totals exhibit significant linear trends over 1896–2023 or 1951–2023. However, monthly nClimgrid indicates *marginally* significant (see Section 2.6)

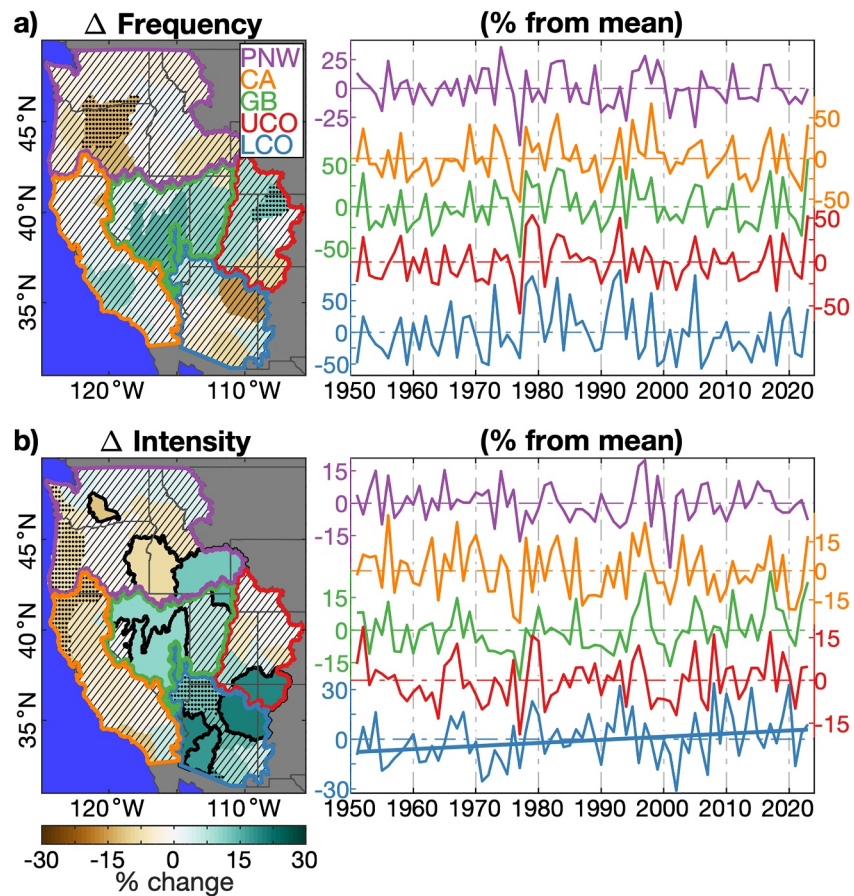


Figure 2. Trends in cool-season wet-day frequency and intensity over 1951–2023. (a) Map of trends and time series plots of the wet-day frequency anomalies. (b) Map of trends and time series plots of wet-day intensity anomalies. Maps show trends (total linear change over 1951–2023 relative to the mean) for each HUC-4 hydrological region. Solid colors, black stippling, and hatching: significant, marginally significant, and insignificant trends, respectively. Thick colored polygons bound the larger HUC-2 regions corresponding to the legend in (a) and as defined in Figure 1 caption. Time series plots express anomalies as percent deviations from the 1951–2023 mean for the 5 HUC-2 regions (colors correspond to the regions as defined in the legend in (a)). Solid trend line: significant trend.

negative trends in southeastern California from 1896 to 2023 and near the coast of Pacific Northwest and northern California from 1951 to 2023 (Figure S11 in Supporting Information S1). Our GHCN data set indicates very similar spatial patterns and magnitudes of 1951–2023 trends as those indicated by nClimGrid (Figures S11b and S11c in Supporting Information S1).

Having established there is no trend in cool-season precipitation totals at the HUC-2 or HUC-4 scales, we now use our daily 1951–2023 data set to evaluate trends in wet-day frequency and mean intensity (Figure 2). Figure 2a shows neutral trends in wet-day frequency across most of the western US, with marginally significant decreases in the central portion of Pacific Northwest and marginally significant increases in northeastern Upper Colorado. There are no significant frequency trends at the larger scale of the HUC-2 regions. Trends in mean wet-day intensity are negative with marginal significance in coastal northern California and Pacific Northwest and significantly negative in one interior subregion of Pacific Northwest (Figure 2b). In Great Basin and Lower Colorado, intensity trends are positive and either significant or marginally significant in most HUC-4 units. At the HUC-2 scale, the only significant intensity trend is an increase of 14% in Lower Colorado.

The regional time series plots in Figure 2 also indicate that the high 2023 precipitation totals in California and Great Basin are due to large positive anomalies in both the frequency and intensity of wet days. The high 2023 precipitation total in Upper Colorado is dominated by wet-day frequency. In each of these regions, the 2023 wet-day frequency ranks in the top-6 on record and is >40% above average (the Upper Colorado anomaly of +48% is

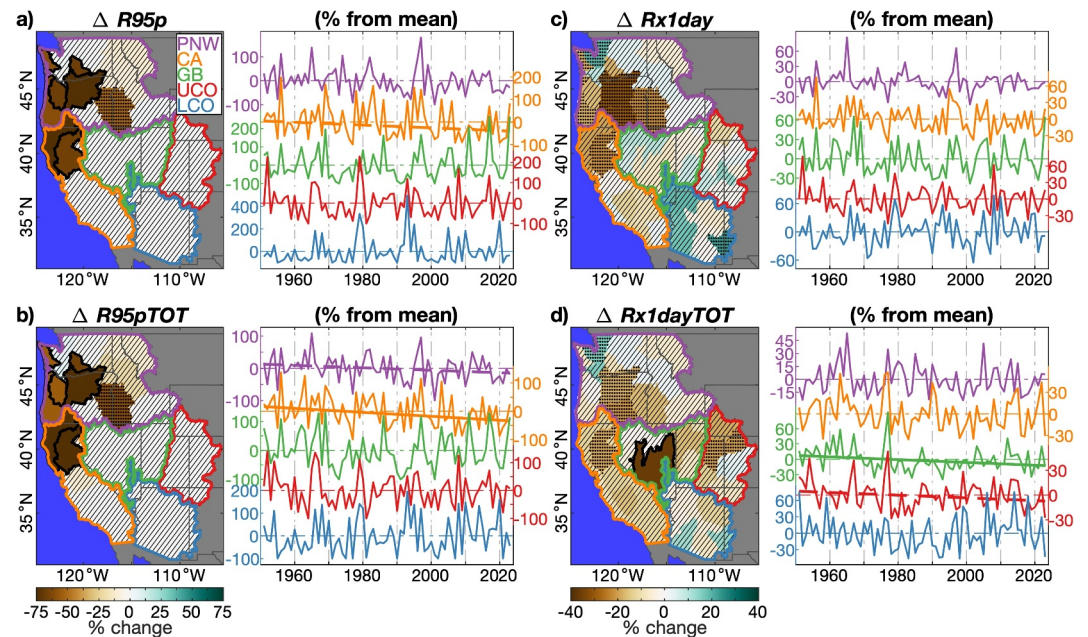


Figure 3. As in Figure 2 but for (a) cool-season precipitation total from days when precipitation exceeded the 95th percentile of all 1951–2023 cool-season wet days ($R95p$), (b) fraction of total cool-season precipitation accounted for by $R95p$ ($R95pTOT$), (c) each cool-season's largest single-day precipitation total ($Rx1day$), and (d) the fraction of total cool-season precipitation accounted for by $Rx1day$ ($Rx1dayTOT$). Color bar under (b) corresponds to (a) and (b). Color bar under (d) corresponds to (c) and (d). Mapped trends are total linear change over 1951–2023 relative to the mean during this period. Anomalies in time-series plots are percent deviations from the 1951–2023 mean. In maps, solid colors, stippling, and hatching: significant, marginally significant, and insignificant trends, respectively. In time series, solid and dashed trend lines: significant and marginally significant trends, respectively.

highest on record) (Figure 2a). Intensity anomalies in 2023 are +22% (3rd on record) in Great Basin and +18% (8th on record) in California (Figure 2b).

Unlike our GHCN data set, daily nClimGrid suggests significant decreases in wet-day intensity in all regions except Lower Colorado (Figure S12 in Supporting Information S1). However, widespread intensity decreases are not well supported by the 321 raw gauge records with the most consistent data coverage over the study period (Figure S2f in Supporting Information S1). We thus interpret the strong declines in inferred wet-day intensity from nClimGrid to be likely artifacts of increased gauge coverage throughout the mountainous interior of the western US over the latter half of the 20th century. As gauge coverage expands, particularly into mountainous areas with higher precipitation frequencies, the likelihood of detecting relatively low daily precipitation totals in a given area increases and this negatively forces the average inferred precipitation intensity (Text S2 in Supporting Information S1).

We next evaluate trends in precipitation contributions on the wettest days. Figure 3a shows trends in cool-season precipitation delivered on days when precipitation exceeded the 95th percentile of all 1951–2023 cool-season wet days ($R95p$). Figure 3b shows trends in the fraction of total cool-season precipitation contributed by $R95p$ ($R95pTOT$). Trends in $R95p$ and $R95pTOT$ are small and insignificant across much of the study region, though there is a broad swath of subregions across northern California and Pacific Northwest where trends are significantly negative, on the order of -60% relative to the 1951–2023 averages. These subregional negative trends drive a marginally significant reduction of 45% in regionally averaged $R95p$ for California and a corresponding significant reduction in $R95pTOT$ of 51% (Figures 3a and 3b). A decline of 27% in Pacific Northwest $R95pTOT$ is marginally significant (Figure 3b).

Similar to the $R95p$ trends, trends in each cool season's largest daily precipitation total ($Rx1day$) are generally negative and insignificant to marginally significant across northern California and southwestern Pacific Northwest (Figure 3c). Outside these areas, trends in $Rx1day$ are weak and of mixed sign. Considering the fractional contribution of each year's $Rx1day$ to total cool-season precipitation ($Rx1dayTOT$), trends are negative across

most of the study area and classified as marginally significant or significant in a number of subregions (Figure 3d). The significant subregional decrease in southwestern Great Basin leads to a significant decrease of 20% in Great Basin's regionally averaged record of *Rx1dayTOT* (Figure 3d). Thus, despite *increases* in Great Basin's average wet-day intensity (Figure 2b), the proportion of Great Basin precipitation delivered by the *wettest* days has declined. In Upper Colorado, a decrease in *Rx1dayTOT* of 12% is marginally significant.

The daily nClimGrid data set also indicates reductions in *R95p* and *Rx1day* across the southwestern portion of Pacific Northwest and northern California, and more generally corroborates our finding that the proportion of cool-season precipitation accounted for by the most intense days has been neutral or declined (Figure S13 in Supporting Information S1). However, the nClimGrid data set suggests the declines in *R95p*, *R95pTOT*, *Rx1day*, and *Rx1dayTOT* are considerably stronger and more widespread than is indicated in our data set. According to the 321 gauges with the most complete records over our study period, significant and marginally significant declines in *R95p*, *R95pTOT*, and *Rx1day* are confined mostly to northern California and the southwestern Pacific Northwest (Figure S14 in Supporting Information S1), more consistent with our results than those from nClimGrid.

Overall, despite anomalously large contributions from very intense precipitation days in 2023, particularly in California and Great Basin, the tendency across much of the western US study area is for the most intense precipitation days to show no trend or to become less intense and less influential on cool-season precipitation totals, particularly in northern California and the southwestern portion of Pacific Northwest.

The lack of intensification of the wettest cool-season days is interesting given that global warming should enhance the atmosphere's moisture-holding capacity and thus the amount of moisture available for precipitation (Trenberth, 1999). We therefore now investigate the relationships between western US extreme precipitation totals their associated moisture fluxes. In Figures 4a and 4b we confirm that extreme precipitation totals, here expressed as *Rx1day*, are strongly and positively influenced by vertically integrated moisture transports (qv) on those wettest days across our study area. However, Figure 4c shows that qv on these days did not increase over 1951–2023 in our study region, and in Great Basin qv on the wettest days decreased significantly. We next decompose qv into anomalies driven by wind velocity (\bar{qv}) and anomalies driven by specific humidity ($q\bar{v}$). Figures 4d–4i indicate that both wind velocity and humidity are important drivers of *Rx1day* across much of the study area. Figures 4f and 4i further indicate significant reductions in \bar{qv} on the wettest days in Great Basin and no change in wettest-day $q\bar{v}$ in any region. When we evaluate moisture transports on each region's wettest three cool-season days, we find significant reductions in \bar{qv} for California and Upper Colorado (Figure S15 in Supporting Information S1). Further, Figure 4c suggests that the qv feeding precipitation on the wettest days of cool-season 2023 was unremarkable, particularly in California, Great Basin, and Upper Colorado, where *Rx1day* anomalies in 2023 were largest (Figure 3b). Results remain consistent when we repeat these analyses using NCEP/NCAR instead of ERA5 (Figure S16 in Supporting Information S1). We interpret results from these qv analyses to suggest that the wettest cool-season storms have not intensified because the moisture transports feeding these storms have not increased.

The neutral or even negative trends in qv on the wettest days (Figures 4c–4f and 4i) are generally representative of trends in qv and total column water (TCW) across the western US and much of the northeastern Pacific Ocean when averaged over the full cool season (Figures 5a and 5b). The vectors in Figure 5a show reduced mean cool-season transports from the North Pacific into Pacific Northwest and northern California. Figure 5b shows insignificant trends in TCW immediately off the coast, likely associated with increases in subsidence over this region (Figure S17 in Supporting Information S1). Thus, even though warming has positively forced evaporative demand, lower-tropospheric specific humidity has not increased enough to maintain constant RH across much of the western US and upwind North Pacific (Figures 5c and 5d). Reduced moisture transports into the northern half of the western US and warming-driven declines in RH in and upwind of the western US are corroborated by the NCEP/NCAR reanalysis (Figure S18 in Supporting Information S1).

In Figure 6 we show that lack of a detectable intensification of cool-season precipitation in the western US thus far is consistent with expectations from the CMIP6. Among 294 simulations from 35 models under the Historical and SSP2-4.5 scenarios, we find that significant simulated trends in *R95p* from 1951 to 2023 are rare for any western US subregion (0%–9% of all model simulations in a given subregion). Although the simulated 1951–2023 trends are relatively weak, the 35-model median *R95p* trends are positive across most of the western US, particularly in Pacific Northwest, Great Basin, and Lower Colorado (Figure 6a). Simulated trends during this period are

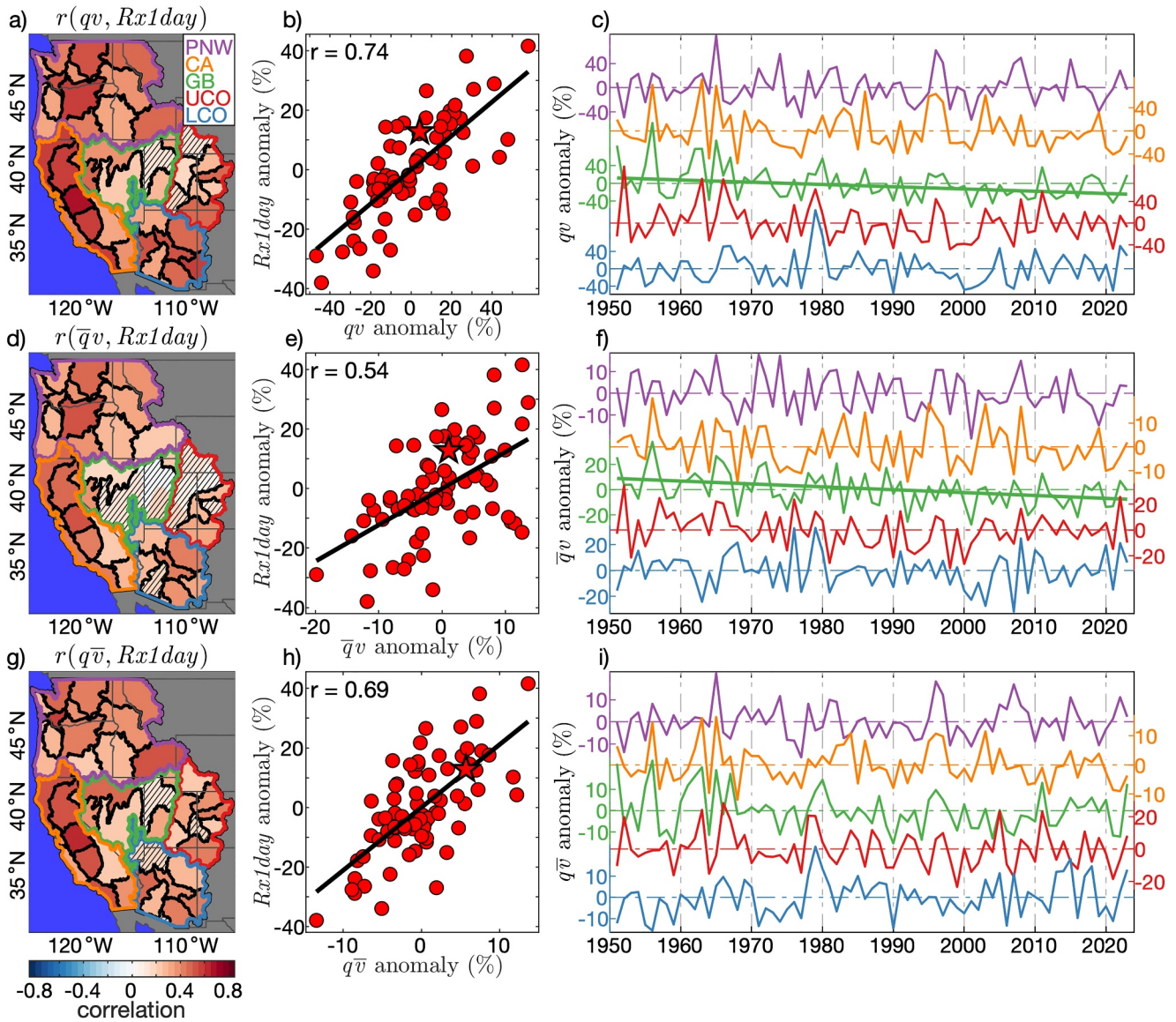


Figure 4. Relationship between precipitation total on the wettest day of each cool-season ($Rx1day$) and integrated moisture transports (qv) on that day, 1951–2023. (a) Pearson's correlation (r) between $Rx1day$ and qv for each HUC-4 hydrological region. (b) Scatter plot of $Rx1day$ versus qv anomalies averaged across all HUC-4 regions (bold line: least-squares regression; star: 2023). (c) Time series of qv anomalies for each of the larger HUC-2 regions (colors correspond to the 5 HUC-2 regions defined in (a)). (d)–(f) Same as (a)–(c) but qv anomalies are driven only by wind velocity anomalies ($\bar{q}v$). (g)–(i) Same as (a)–(c) but qv anomalies are driven only by specific humidity anomalies ($q\bar{v}$). Anomalies expressed as percent deviation from 1951 to 2023 mean. Anomalies in $\bar{q}v$ and $q\bar{v}$ are relative to the mean of qv . In maps, solid and hatching: significant and insignificant correlations, respectively. In scatter plots all correlations are significant. In time series, solid trend lines: significant.

generally similar for $R95pTOT$ and weaker for $Rx1day$ and $Rx1dayTOT$ (Figure S19 in Supporting Information S1).

In Figure 6b, we show the 35-model median and spread of 21-year running mean $R95p$ anomalies from 1850 to 2100 under the Historical and SSP2-4.5 scenarios for each HUC-2 region. The simulated anthropogenic increases are strongest in Pacific Northwest, Upper Colorado, and Great Basin, where the 35-model median $R95p$ anomalies averaged over 2080–2100 are >40% above the 1951–2023 mean. In California and Lower Colorado, projected trends are weaker but consistently positive across models. Results are similar for $R95pTOT$ and considerably weaker for $Rx1day$ and $Rx1dayTOT$ (Figure S19 in Supporting Information S1).

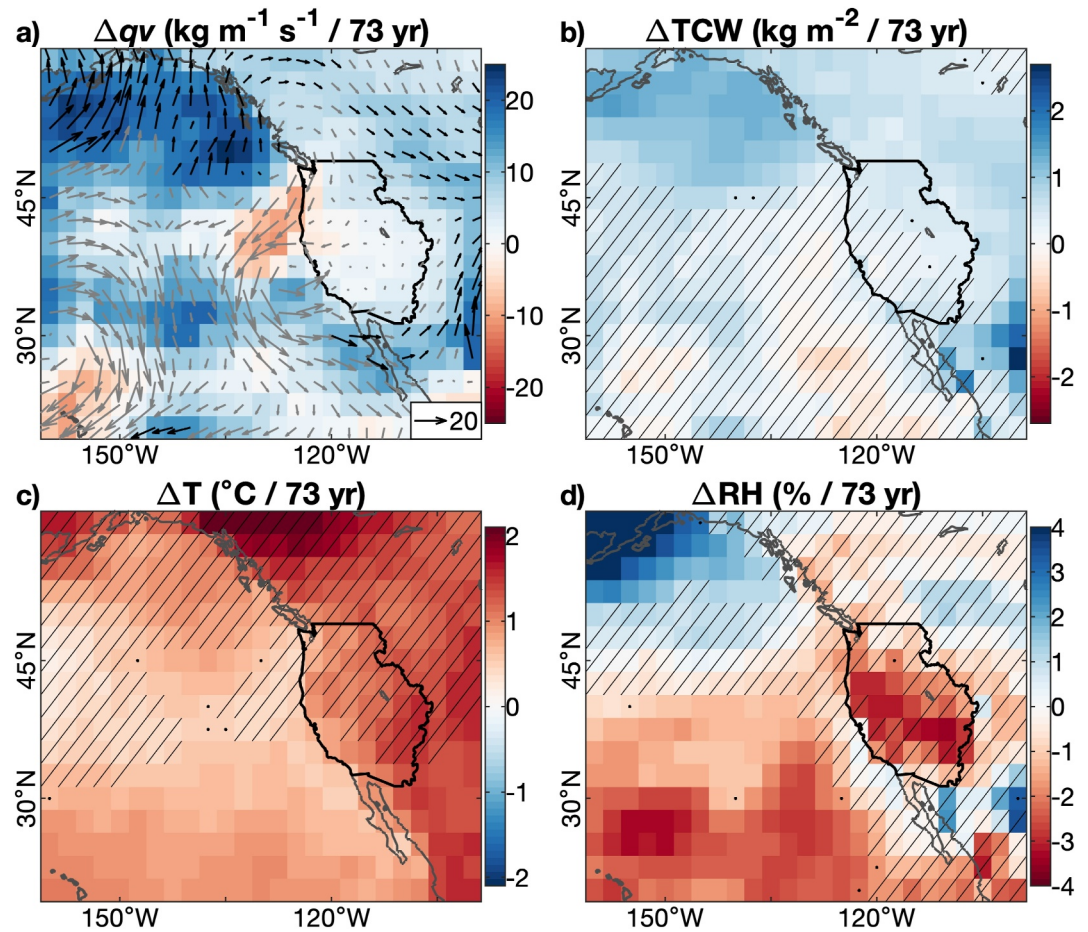


Figure 5. Linear trends in cool-season atmospheric conditions over the North Pacific and western North America, 1951–2023, as represented by the ERA5 reanalysis. (a) Vertically integrated vapor transports (qv) from the surface to 300 hPa (background: absolute change; vectors: directional change). (b) Change in total column water. (c) Lower tropospheric (surface to 500 hPa) temperature (T). (d) Lower tropospheric relative humidity (RH). In (c) and (d), vertical means of T and RH are weighted by specific humidity to reflect conditions where water vapor is present. In (a), black vector arrows: significant qv trends; gray vector arrow: insignificant or marginally significant trends. In (b)–(d), solid colors, black dots, and hatching: significant, marginally significant, and insignificant trends, respectively. Black polygon bounds our western US study region.

We next perform a TOE analysis to determine when models project anthropogenic forcing to consistently alter the statistical distribution of cool-season $R95p$ under the SSP2-4.5 scenario. In Figure 6b, each colored dot above a HUC-2 time series indicates when a given model's $R95p$ takes on a significantly different ($p < 0.1$) distribution from that established over 1851–1950. For Pacific Northwest, Great Basin, and Upper Colorado, the majority of models simulate emergence by the 2050s. In California, the 35-model median TOE is 2080, though inter-model spread is large; four models simulate emergence prior to 2050 and 12 models (34%) simulate no 21st-century emergence. For California and Upper Colorado, recent assessments have ranked the CMIP6 models in terms of the realism with which they simulate local climate (Krantz et al., 2022; Pierce et al., 2022). Repeating our analysis with only the CMIP6 models recently ranked as among each region's top-10 performers, the median TOE is unchanged for Upper Colorado but advances from 2080 to 2065 for California. Projected trends are weakest for Lower Colorado, where 21 models (60%) do not simulate emergence prior to 2100, meaning no multi-model median TOE for that region (Figure 6b).

Under the more aggressive SSP5-8.5 emissions scenario, the 35-model median TOE advances to the 2040s for Pacific Northwest and Great Basin, 2049 in Upper Colorado, 2067 in California, and 2088 in Lower Colorado (Figure S20 in Supporting Information S1). Considering the 10 highest ranked models for California, the SSP5-8.5 median TOE advances to 2055. In addition, models indicate a considerable influence of internal climate

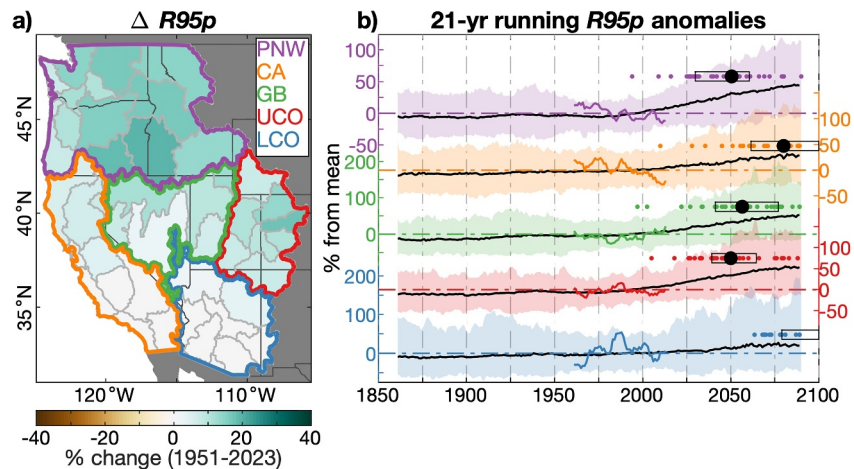


Figure 6. Coupled Model Intercomparison Project (CMIP6) trends in cool-season precipitation total from days when precipitation exceeded the 95th percentile of all 1951–2023 cool-season wet days ($R95p$) according to 35 CMIP6 models under the Historical and SSP2-4.5 scenarios. (a) All-model median linear change over 1951–2023 for each HUC-4 hydrological subregion. Mapped trends are total linear change over 1951–2023 relative to the mean during this period. (b) 21-year running $R95p$ anomalies expressed as percent deviations from the 1951–2023 mean for each HUC-2 region. Bold black time series and colored shading: all-model median and spread among all realizations, respectively; bold colored time series: observed. Colored dots: each model's median time-of-emergence. Black dot and rectangle: all-model median and interquartiles, respectively. Rectangles extending to 2100: $\geq 25\%$ of models do not indicate emergence by 2100. No black dot: $< 50\%$ of models indicate emergence by 2100.

variability on TOE, which is not shown in Figure 6b (or Figures S19 and S20 in Supporting Information S1). Considering the 100 projections by the CESM2 large ensemble under the SSP3-7.0 scenario, we find that while the 100-realization median TOE for $R95p$ in California is 2082, 3 realizations indicate a TOE prior to 2050 and 28 indicate no 21st-century emergence (Figure S21 in Supporting Information S1).

Finally, how do simulated trends in precipitation extremes compare to those observed thus far? Considering the 294 realizations of CMIP6 Historical simulations extended with SSP2-4.5, 254 realizations extended with SSP5-8.5, and 100 realizations extended with SSP3-7.0 from the CESM2 large ensemble, the observed declines in cool-season $R95p$ in Pacific Northwest and California are near the lower edge of the distribution of simulated trends over 1951–2023 (Figure 7). Of the 648 simulated $R95p$ trends evaluated, only 3 are more negative than observed in Pacific Northwest (produced by 3 of the 35 models) and 11 are more negative than observed in California (produced by 4 models). Results are essentially identical when time series are standardized to have the same variance (Figure S22 in Supporting Information S1) and the observed negative trends are even closer to the lower edge of the CMIP6 distribution when we consider $R95p_{TOT}$ instead of $R95p$ (Figure S23 in Supporting Information S1). Importantly, the small number simulations of trends more negative than those observed in Pacific Northwest and California are from large ensembles (e.g., ≥ 10 simulations). This underscores the importance of assessing large ensembles when evaluating discrepancies between observed and modeled climate trends and suggests that more models may be capable of simulating trends similar to those observed than what is presented in Figure 7.

4. Discussion and Conclusions

Across the western US, extremely high cool-season precipitation totals in 2023 were driven by a combination of a high proportion of days with precipitation (frequency) and large precipitation totals on these days (intensity). In Great Basin and California, the contribution from very large single-day totals was particularly high. In California, the high precipitation intensity in 2023 was in contrast to small reductions in intensity from 1951 to 2023 that were marginally significant in northern California and part of larger-scale reductions across much of western Pacific Northwest. On the other hand, mean cool-season precipitation intensity increased over 1951–2023 across much of the Great Basin region, though these trends were representative of the average wet day and not of the wettest days. In the Lower Colorado region, 2023 precipitation intensity was not anomalous, but that is the only large region where significant increases in mean precipitation intensity occurred. Additionally, our study highlights the

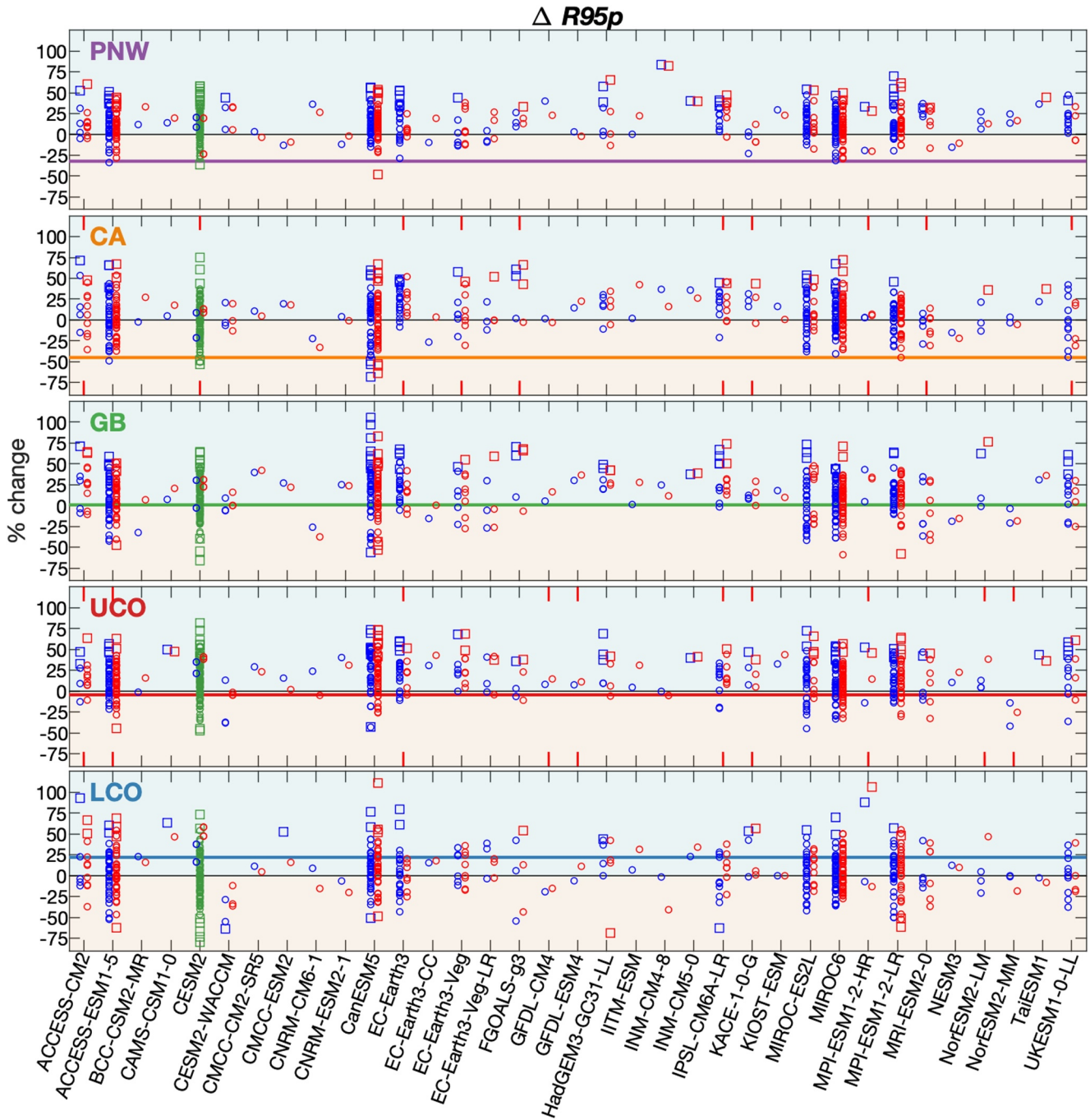


Figure 7. Trends in precipitation totals from days exceeding the 95th percentile of all 1951–2023 cool-season wet days ($R95p$) for the 5 HUC-2 regions according to observations (horizontal colored lines) and simulations by 35 CMIP6 models (blue, red, and green circles and squares) over 1951–2023. Trends expressed as total linear change relative to the 1951–2023 mean. Each circle or square represents a single simulated trend using output from the CMIP6 Historical scenario through 2014 and extending through 2023 with output from (blue) SSP2-4.5, (red) SSP5-8.5, or (green) SSP3-7.0 scenario. Squares: statistically significant ($p < 0.1$) simulated trends. Regional abbreviations defined in Figure 1. Red tick marks in the CA and UCO panels indicate the models ranked as among the top-10 by Krantz et al. (2022) and Pierce et al. (2022), respectively. Data for the SSP3-7.0 scenario come from the CESM2 100-member large ensemble.

importance a stable network of long, continuous gauge records in assessments of trends in precipitation intensity. For example, the daily NOAA nClimGrid data set, which uses a larger gauge network that generally increased in density over the latter half of the 20th century, suggests far more widespread decreases in precipitation intensity than are apparent in our data set or among the most complete gauge records.

Both the observed geographic patterns of precipitation anomalies in 2023 as well as the 1951–2023 trends are inconsistent with the expected effect of anthropogenic greenhouse-gas forcing on wet extremes in the western US. First, the observed trends toward reduced precipitation intensity in the northwestern US and increases in the southwestern US are opposite from the fingerprint expected from anthropogenic forcing alone. Further, in Mediterranean climate regions globally, models project increases in precipitation intensity to be counterbalanced by reductions in precipitation frequency, especially in California (Polade et al., 2014, 2017). Gershunov et al. (2019) showed that in California and Pacific Northwest, these projected trends manifest specifically as intensification of the wettest days associated with atmospheric rivers. Thus, models project the wettest days to make up an increasingly large share of the total cool-season precipitation on the US west coast, but no such redistribution of daily precipitation totals has been observed thus far.

The primary mechanism by which anthropogenic forcing is projected to intensify western US cool-season precipitation is via enhanced atmospheric water vapor. However, the reanalysis data sets we investigated show no increase in cool-season vapor transports into the western US from the North Pacific thus far, including on the wettest days over the 1951–2023 study period. At least part of the reason is that atmospheric circulation trends appear to have prevented warming-driven atmospheric moistening in the cool season and have also slowed westerly wind velocities into the western US. These results are consistent with a previously observed reduction in the occurrences of atmospheric circulation patterns associated with winter precipitation in California over 1948–2021 (Guirguis et al., 2023). The results also extend the temporal context of previously observed 1980–2016 reductions of mean cool-season precipitable water across much of the western US as well as moisture transports associated with atmospheric rivers in California (Dettinger et al., 2018; Kunkel et al., 2020).

Should we expect western US precipitation extremes to already reflect the influence of anthropogenic forcing? On the whole, CMIP6 models suggest that forced increases in precipitation intensity should thus far be weak relative to the large range of natural variability across much of this region. In California, where 2023 precipitation totals were particularly large but so is the range of variability, we find that CMIP6 models generally do not project an increase in the intensity of the wettest days to become detectable until the 2060s or later, even under the very high SSP5-8.5 emissions scenario, though the median TOE among 10 models previously found to have the highest fidelity in California (Krantz et al., 2022) is approximately a decade sooner. Our finding that climate models generally do not simulate detectable intensification of western US cool-season precipitation thus far is consistent with prior results based on a much smaller ensemble of simulations (King et al., 2015; Tseng et al., 2022). Besides large natural variability in western US precipitation intensity, anthropogenic aerosols may have also counteracted the expected positive greenhouse-gas forcing on precipitation intensity and atmospheric moisture content over the western US thus far (Baek & Lora, 2021; Risser et al., 2024).

A caveat to our CMIP6 analyses is that model biases could systematically under- or over-represent the capacity for forced or unforced trends in extreme precipitation. For example, low spatial resolution leads to positive biases in regional precipitation frequencies and prevents realistic representation of important features of orographic precipitation such as updraft rates and sharp precipitation gradients on windward versus leeward sides of mountains (Rahimi et al., 2024). Rahimi et al. (2024) recently produced dynamically downscaled simulations for 14 CMIP6 models for the western US at 9-km resolution covering 1980–2014 from the Historical Scenario and 2015–2100 from the SSP3-7.0 scenario. Comparing the dynamically downscaled projections to their corresponding original CMIP6 realizations, we find that projected relative changes in $R95p$ calculated from the dynamically downscaled simulations have a weak tendency to be smaller than those inferred from the original CMIP6 projections, particularly in Pacific Northwest (Figure S24 in Supporting Information S1). This suggests that our CMIP6-based assessments of when precipitation intensification becomes detectable could be biased early, though we cannot assess this definitively in part because the Rahimi et al. (2024) simulations begin in 1980 and thus do not include a historical baseline period. Future efforts should evaluate how downscaling techniques may affect model-based expectations of when precipitation intensification is likely to become statistically detectable. In addition, while downscaling can provide critical spatiotemporal details not available from coarser global climate models, it does not resolve more fundamental problems with how CMIP6 models may represent the global climate. In the equatorial Pacific, for example, climate models tend to erroneously simulate a double intertropical convergence zone, and biases in ocean-atmosphere coupling lead to misrepresentation of geographic gradients in sea surface temperature, humidity, wind speed, and precipitation (Baldwin et al., 2021; Lin, 2007; Seager et al., 2019). Given that western US cool-season precipitation is particularly sensitive to the coupled ocean-atmosphere dynamics of the tropical Pacific, model biases in that region represent a large source of

uncertainty in the future of western US precipitation intensity that cannot be resolved with regional downscaling (Schmidt & Grise, 2021).

According to the CMIP6 ensemble median, precipitation intensification is projected to become detectable in the 2040s–2060s in Pacific Northwest but not before the 2090s in Lower Colorado, which opposes the geographic pattern of observed intensity trends thus far. Moreover, the observed *negative* trends in daily precipitation extremes in Pacific Northwest and California over 1951–2023 are near the lower bounds of the full range of the 648 simulated trends under historical forcings that we evaluated. If climate models accurately simulate the capacity for natural decadal variability in western US precipitation intensity, then the observed declines in Pacific Northwest and California are simply highly improbable and likely to reverse. On the other hand, precipitation trends have been found to lie outside or on the fringe of modeled trend distributions in other regions as well (Bishop et al., 2019; Varuolo-Clarke et al., 2021). Further, the historical reductions in western US RH shown in Figure 5d are part of a reduction in humidity across arid and semi-arid regions globally that climate models appear systematically incapable of simulating under historical forcings (Simpson et al., 2023). This in combination with the model limitations discussed above highlights the possibility that climate models mischaracterize the effects of natural multidecadal variability and/or anthropogenic forcing on western US precipitation.

Based on the totality of observational and modeling evidence, we conclude it is probably premature to consider anthropogenic forcing as an important driver of extremely wet cool-season anomalies in the western US to date. This conclusion is predicated partly on the finding that the moisture transports feeding the strongest cool-season storms in the western US have not increased and were not particularly strong in 2023, at odds with the thermodynamic mechanism through which greenhouse-gas forcing is expected to intensify precipitation. However, the large number of simulations we evaluated also indicate that natural climate variability will play a heavy hand in dictating the exact timing of this detectability. Natural variability could be the driver of the inconsistency between observed trends and those represented by the median of many simulated responses to anthropogenic forcing, and natural variability could thus drive a future intensification that is consistent with or exceeds the median simulated trend. Further, lack of an observed multi-decade intensification trend thus far, or model simulations indicating the timing of emergence should still be decades off, do not negate the possibility that anthropogenic forcing could soon enhance, or has already enhanced, the moisture delivered by an individual event or in an individual year (Huang & Swain, 2022; Michaelis et al., 2022). It will likely be in rare, individual storms on a backdrop of anomalous circulation characteristics that thermodynamically enhanced evaporation rates from the Pacific can manifest as intensified precipitation totals in the western US. It could thus take years or decades for the integrated effects of these relatively rare events to result in a statistical emergence based on the traditional definition of emergence that we adopted for this study. Thus, the sound science underpinning projections of intensified precipitation across most land area globally (Pfahl et al., 2017), in combination with the straightforward expectation that warming will continue to weaken the western US snowpack reservoir (Gottlieb & Mankin, 2024; Livneh & Badger, 2020; Shulgina et al., 2023), should be considered as western US decision makers weigh opportunities to enhance resilience to increasingly large and rapid runoff events and their associated flood hazards.

Data Availability Statement

All data are publicly available from the following sources: Daily GCHN gauge precipitation (Menne, Durre, Korzeniewski, et al., 2012): <https://doi.org/10.7289/V5D21VHZ>. The daily gridded precipitation data set and the underlying gap-filled gauge records developed for this study (Williams, 2024): <https://doi.org/10.5061/dryad.c866t1gfp>. NOAA nClimgrid monthly precipitation (Vose et al., 2014): <https://www.ncei.noaa.gov/access/metadata/landing-page/bin/iso?id=gov.noaa.ncdc:C00332>. NOAA nClimgrid daily precipitation (Durre, Squires, et al., 2022): <https://www.ncei.noaa.gov/products/land-based-station/ncimgrid-daily>. Climate Prediction Center daily precipitation (CPC, 2008): <https://psl.noaa.gov/data/gridded/data.unified.daily.conus.html>. NCEP/NCAR reanalysis (NCEP-NCAR, 1996): <https://psl.noaa.gov/data/reanalysis/reanalysis.shtml>. ERA5 reanalysis (ECMWF, 2020): <https://www.ecmwf.int/en/forecasts/dataset/ecmwf-reanalysis-v5>. Boundaries of USGS hydrological units (Tijerina, 2019): <http://www.hydroshare.org/resource/b832a6c2f96541808444ec9562c5247e>. CMIP6 data (ESGF, 2024): <https://esgf-node.lnl.gov/search/cmip6/>. Dynamically downscaled CMIP6 data (Rahimi, 2024): <https://registry.opendata.aws/wrf-cmip6/>. CESM2 Large Ensemble data (NCAR, 2022): <https://www.cesm.ucar.edu/community-projects/lens2>.

Acknowledgments

We thank five reviewers for thorough and constructive feedback on our original submission. We acknowledge funding from California's Department of Water Resources (agreement # 4600014359; APW, KJA), the Zegar Family Foundation (APW, HL), the Gordon and Betty Moore Foundation (APW, # 11974), the MacArthur Foundation (APW), the Department of the Interior Southwest Climate Adaptation Science Center, which is managed by the USGS National Climate Adaptation Science Center (G18AC00320; AG, RESC), and the David and Lucile Packard Foundation (KAM).

References

Allan, R. P., & Soden, B. J. (2008). Atmospheric warming and the amplification of precipitation extremes. *Science*, 321(5895), 1481–1484. <https://doi.org/10.1126/science.1160787>

Baek, S. H., & Lora, J. M. (2021). Counterbalancing influences of aerosols and greenhouse gases on atmospheric rivers. *Nature Climate Change*, 11(11), 958–965. <https://doi.org/10.1038/s41558-021-01166-8>

Baldwin, J. W., Atwood, A. R., Vecchi, G. A., & Battisti, D. S. (2021). Outsize influence of Central American orography on global climate. *AGU Advances*, 2(2), e2020AV000343. <https://doi.org/10.1029/2020AV000343>

Bishop, D. A., Williams, A. P., Seager, R., Fiore, A. M., Cook, B. I., Mankin, J. S., et al. (2019). Investigating the causes of increased twentieth-century fall precipitation over the Southeastern United States. *Journal of Climate*, 32(2), 575–590. <https://doi.org/10.1175/JCLI-D-18-0244.1>

CPC. (2008). CPC unified gauge-based analysis of daily precipitation over CONUS (version 1) [Dataset]. *NOAA Physical Sciences Laboratory*. Retrieved from <https://psl.noaa.gov/data/gridded/data.unified.daily.conus.html>

Daly, C., Doggett, M. K., Smith, J. I., Olson, K. V., Halbleib, M. D., Dimcovic, Z., et al. (2021). Challenges in observation-based mapping of daily precipitation across the conterminous United States. *Journal of Atmospheric and Oceanic Technology*, 38(11), 1979–1992. <https://doi.org/10.1175/JTECH-D-21-0054.1>

Daly, C., Halbleib, M., Smith, J. I., Gibson, W. P., Doggett, M. K., Taylor, G. H., et al. (2008). Physiographically sensitive mapping of climatological temperature and precipitation across the conterminous United States. *International Journal of Climatology*, 28(15), 2031–2064. <https://doi.org/10.1002/joc.1688>

Danabasoglu, G., Lamarque, J.-F., Bacmeister, J., Bailey, D. A., DuVivier, A. K., Edwards, J., et al. (2020). The community earth system model version 2 (CESM2). *Journal of Advances in Modeling Earth Systems*, 12(2), e2019MS001916. <https://doi.org/10.1029/2019MS001916>

Dettinger, M. D. (2016). Historical and future relations between large storms and droughts in California. *San Francisco Estuary and Watershed Science*, 14(2), 1–21. <https://doi.org/10.15447/sfews.2016v14iss2art1>

Dettinger, M. D., Ralph, F. M., & Rutz, J. J. (2018). Empirical return periods of the most intense vapor transports during historical atmospheric river landfalls on the US West Coast. *Journal of Hydrometeorology*, 19(8), 1363–1377. <https://doi.org/10.1175/JHM-D-17-0247.1>

Dong, S., Sun, Y., Li, C., Zhang, X., Min, S.-K., & Kim, Y.-H. (2021). Attribution of extreme precipitation with updated observations and CMIP6 simulations. *Journal of Climate*, 34(3), 871–881. <https://doi.org/10.1175/JCLI-D-19-1017.1>

Durre, I., Arguez, A., SchreckIII, C. J., Squires, M. F., & Vose, R. S. (2022). Daily high-resolution temperature and precipitation fields for the contiguous United States from 1951 to present. *Journal of Atmospheric and Oceanic Technology*, 39(12), 1837–1855. <https://doi.org/10.1175/JTECH-D-22-0024.1>

Durre, I., Squires, M. F., Vose, R. S., Arguez, A., Gross, W. S., Rennie, J. R., & Schreck, C. J. (2022). NOAA's nClimGrid-Daily Version 1 – Daily gridded temperature and precipitation for the Contiguous United States since 1951 (Version 1) [Dataset]. *NOAA National Centers for Environmental Information*. <https://doi.org/10.25921/c4gt-r169>

ECMWF. (2020). ECMWF reanalysis v5 (ERA5) (version 5) [Dataset]. *Copernicus Climate Data Store*. Retrieved from <https://www.ecmwf.int/en/forecasts/dataset/ecmwf-reanalysis-v5>

ESGF. (2024). Earth system grid federation database of CMIP6 data (version 1) [Dataset]. *Earth System Grid Federation*. Retrieved from <https://aims2.llnl.gov/search/cmip6/>

Eyring, V., Bony, S., Meehl, G. A., Senior, C. A., Stevens, B., Stouffer, R. J., & Taylor, K. E. (2016). Overview of the coupled model inter-comparison project phase 6 (CMIP6) experimental design and organization. *Geoscientific Model Development*, 9(5), 1937–1958. <https://doi.org/10.5194/gmd-9-1937-2016>

Fischer, E. M., Sedláček, J., Hawkins, E., & Knutti, R. (2014). Models agree on forced response pattern of precipitation and temperature extremes. *Geophysical Research Letters*, 41(23), 8554–8562. <https://doi.org/10.1002/2014GL062018>

Gershunov, A., Shulgina, T., Clemesha, R. E. S., Guirguis, K., Pierce, D. W., Dettinger, M. D., et al. (2019). Precipitation regime change in Western North America: The role of atmospheric rivers. *Scientific Reports*, 9(1), 9944. <https://doi.org/10.1038/s41598-019-46169-w>

Giorgi, F., Im, E.-S., Coppola, E., Diffenbaugh, N. S., Gao, X. J., Mariotti, L., & Shi, Y. (2011). Higher hydroclimatic intensity with global warming. *Journal of Climate*, 24(20), 5309–5324. <https://doi.org/10.1175/2011JCLI3979.1>

Gottlieb, A. R., & Mankin, J. S. (2024). Evidence of human influence on Northern Hemisphere snow loss. *Nature*, 625(7994), 293–300. <https://doi.org/10.1038/s41586-023-06794-y>

Guirguis, K., Gershunov, A., Hatchett, B., Shulgina, T., DeFlorio, M. J., Subramanian, A. C., et al. (2023). Winter wet–dry weather patterns driving atmospheric rivers and Santa Ana winds provide evidence for increasing wildfire hazard in California. *Climate Dynamics*, 60(5–6), 1729–1749. <https://doi.org/10.1007/s00382-022-06361-7>

Harp, R. D., & Horton, D. E. (2022). Observed changes in daily precipitation intensity in the United States. *Geophysical Research Letters*, 49(19), e2022GL099955. <https://doi.org/10.1029/2022GL099955>

Hawkins, E., Anderson, B., Diffenbaugh, N., Mahlstein, I., Betts, R., Hegerl, G., et al. (2014). Uncertainties in the timing of unprecedented climates. *Nature*, 511(7507), E3–E5. <https://doi.org/10.1038/nature13523>

Hegerl, G. C., Black, E., Allan, R. P., Ingram, W. J., Polson, C., Trenberth, K. E., et al. (2015). Challenges in quantifying changes in the global water cycle. *Bulletin of the American Meteorological Society*, 96(7), 1097–1115. <https://doi.org/10.1175/bams-d-13-00212.1>

Hersbach, H., Bell, B., Berrisford, P., Hirahara, S., Horányi, A., Muñoz-Sabater, J., et al. (2020). The ERA5 global reanalysis. *Quarterly Journal of the Royal Meteorological Society*, 146(730), 1999–2049. <https://doi.org/10.1002/qj.3803>

Huang, X., & Stevenson, S. (2021). Connections between mean North Pacific circulation and western US precipitation extremes in a warming climate. *Earth's Future*, 9(6), e2020EF001944. <https://doi.org/10.1029/2020EF001944>

Huang, X., & Swain, D. L. (2022). Climate change is increasing the risk of a California megaflood. *Science Advances*, 8(31), eabq0995. <https://doi.org/10.1126/sciadv.abq0995>

Kalnay, E., Kanamitsu, M., Kistler, R., Collins, W., Deaven, D., Gandin, L., et al. (1996). The NCEP/NCAR 40-year reanalysis project. *Bulletin of the American Meteorological Society*, 77(3), 437–471. <https://doi.org/10.1175/1520-0477%281996%29077%3C0437%3ATNYRP%3E2.0.CO%3B2>

Kay, J. E., Deser, C., Phillips, A., Mai, A., Hannay, C., Strand, G., et al. (2015). The community Earth system model (CESM) large ensemble project: A community resource for studying climate change in the presence of internal climate variability. *Bulletin of the American Meteorological Society*, 96(8), 1333–1349. <https://doi.org/10.1175/BAMS-D-13-00255.1>

King, A. D., Donat, M. G., Fischer, E. M., Hawkins, E., Alexander, L. V., Karoly, D. J., et al. (2015). The timing of anthropogenic emergence in simulated climate extremes. *Environmental Research Letters*, 10(9), 094015. <https://doi.org/10.1088/1748-9326/10/9/094015>

Krantz, W., Pierce, D., Goldenson, N., & Cayan, D. (2022). *Memorandum on evaluating global climate models for studying regional climate change in California (California energy commission's applied research grant EPC-20-006: Development of climate projections for California*

- and identification of priority projections No. EPC-20-006) (p. 24). Scripps Institution of Oceanography: California Energy Commission. Retrieved from https://www.energy.ca.gov/media/7264oj0D_xpDH
- Kunkel, K. E., Karl, T. R., Squires, M. F., Yin, X., Stegall, S. T., & Easterling, D. R. (2020). Precipitation extremes: Trends and relationships with average precipitation and precipitable water in the contiguous United States. *Journal of Applied Meteorology and Climatology*, 59(1), 125–142. <https://doi.org/10.1175/JAMC-D-19-0185.1>
- Lehner, F., Deser, C., & Terray, L. (2017). Toward a new estimate of “time of emergence” of anthropogenic warming: Insights from dynamical adjustment and a large initial-condition model ensemble. *Journal of Climate*, 30(19), 7739–7756. <https://doi.org/10.1175/JCLI-D-16-0792.1>
- Liepert, B. G., Feichter, J., Lohmann, U., & Roeckner, E. (2004). Can aerosols spin down the water cycle in a warmer and moister world? *Geophysical Research Letters*, 31(6). <https://doi.org/10.1029/2003GL019060>
- Lin, J.-L. (2007). The double-ITCZ problem in IPCC AR4 coupled GCMs: Ocean–atmosphere feedback analysis. *Journal of Climate*, 20(18), 4497–4525. <https://doi.org/10.1175/JCLI4272.1>
- Livneh, B., & Badger, A. M. (2020). Drought less predictable under declining future snowpack. *Nature Climate Change*, 10(5), 452–458. <https://doi.org/10.1038/s41558-020-0754-8>
- Luce, C. H., Abatzoglou, J. T., & Holdren, Z. A. (2013). The missing mountain water: Slower westerlies decrease orographic enhancement in the Pacific Northwest USA. *Science*, 342(6164), 1360–1364. <https://doi.org/10.1126/science.1242335>
- Mahlstein, I., Portmann, R. W., Daniel, J. S., Solomon, S., & Knutti, R. (2012). Perceptible changes in regional precipitation in a future climate. *Geophysical Research Letters*, 39(5), L05701. <https://doi.org/10.1029/2011GL050738>
- Marquardt Collow, A. B., Shields, C. A., Guan, B., Kim, S., Lora, J. M., McClenny, E. E., et al. (2022). An overview of ARTMIP’s Tier 2 Reanalysis Intercomparison: Uncertainty in the detection of atmospheric rivers and their associated precipitation. *Journal of Geophysical Research: Atmospheres*, 127(8), e2021JD036155. <https://doi.org/10.1029/2021JD036155>
- Marshall, A. M., Abatzoglou, J. T., Rahimi, S., & Hall, A. (2024). California’s 2023 snow deluge: Contextualizing an extreme snow year against future climate change. *Proceedings of the National Academy of Sciences USA*, 121(20), e2320600121. <https://doi.org/10.1073/pnas.2320600121>
- Menne, M. J., Durre, I., Korzeniewski, B., McNeill, S., Thomas, K., Yin, X., et al. (2012). Global historical climatology network - daily (GHCN-Daily) (version 3). [Dataset]. NOAA National Climatic Data Center. <https://doi.org/10.7289/V5D21VHZ>
- Menne, M. J., Durre, I., Vose, R. S., Gleason, B. E., & Houston, T. G. (2012). An overview of the global historical climatology network-daily database. *Journal of Atmospheric and Oceanic Technology*, 29(7), 897–910. <https://doi.org/10.1175/JTECH-D-11-00103.1>
- Michaelis, A. C., Gershunov, A., Weyant, A., Fish, M. A., Shulgina, T., & Ralph, F. M. (2022). Atmospheric river precipitation enhanced by climate change: A case study of the storm that contributed to California’s Oroville Dam crisis. *Earth’s Future*, 10(3), e2021EF002537. <https://doi.org/10.1029/2021EF002537>
- Min, S.-K., Zhang, X., Zwiers, F. W., & Hegerl, G. C. (2011). Human contribution to more-intense precipitation extremes. *Nature*, 470(7334), 378–381. <https://doi.org/10.1038/nature09763>
- Myhre, G., Forster, P. M., Samsel, B. H., Hodnebrog, Ø., Sillmann, J., Aalbergsjø, S. G., et al. (2017). PDRMIP: A precipitation driver and response model intercomparison project—Protocol and preliminary results. *Bulletin of the American Meteorological Society*, 98(6), 1185–1198. <https://doi.org/10.1175/BAMS-D-16-0019.1>
- NCAR. (2022). CESM2 large ensemble community project (LENS2) [Dataset]. National Center for Atmospheric Research Climate Data Gateway. Retrieved from <https://www.cesm.ucar.edu/community-projects/lens2/data-sets>
- NCEP-NCAR. (1996). NCEP-NCAR reanalysis 1 (version 1) [Dataset]. NOAA Physical Sciences Laboratory. Retrieved from <https://psl.noaa.gov/data/reanalysis/reanalysis.shtml>
- Norris, J., Chen, G., & Neelin, J. D. (2019). Thermodynamic versus dynamic controls on extreme precipitation in a warming climate from the community Earth system model large ensemble. *Journal of Climate*, 32(4), 1025–1045. <https://doi.org/10.1175/JCLI-D-18-0302.1>
- Norris, J., Hall, A., Chen, D., Thackeray, C. W., & Madakumbura, G. D. (2021). Assessing the representation of synoptic variability associated with California extreme precipitation in CMIP6 models. *Journal of Geophysical Research: Atmospheres*, 126(6), e2020JD033938. <https://doi.org/10.1029/2020JD033938>
- O’Gorman, P. A. (2015). Precipitation extremes under climate change. *Current Climate Change Reports*, 1(2), 49–59. <https://doi.org/10.1007/s40641-015-0009-3>
- O’Gorman, P. A., & Schneider, T. (2009). The physical basis for increases in precipitation extremes in simulations of 21st-century climate change. *Proceedings of the National Academy of Sciences USA*, 106(35), 14773–14777. <https://doi.org/10.1073/pnas.0907610106>
- O’Neill, B. C., Tebaldi, C., Van Vuuren, D. P., Eyring, V., Friedlingstein, P., Hurtt, G., et al. (2016). The scenario model intercomparison project (ScenarioMIP) for CMIP6. *Geoscientific Model Development*, 9, 3461–3482. <https://doi.org/10.5194/gmd-9-3461-2016>
- Pendergrass, A. G., & Hartmann, D. L. (2012). Global-mean precipitation and black carbon in AR4 simulations. *Geophysical Research Letters*, 39(1), L01703. <https://doi.org/10.1029/2011GL050067>
- Pendergrass, A. G., Knutti, R., Lehner, F., Deser, C., & Sanderson, B. M. (2017). Precipitation variability increases in a warmer climate. *Scientific Reports*, 7(1), 17966. <https://doi.org/10.1038/s41598-017-17966-y>
- Peterson, T. C., & Manton, M. J. (2008). Monitoring changes in climate extremes: A tale of international collaboration. *Bulletin of the American Meteorological Society*, 89(9), 1266–1271. <https://doi.org/10.1175/2008BAMS2501.1>
- Pfahl, S., O’Gorman, P. A., & Fischer, E. M. (2017). Understanding the regional pattern of projected future changes in extreme precipitation. *Nature Climate Change*, 7(6), 423–427. <https://doi.org/10.1038/nclimate3287>
- Pierce, D. W., Cayan, D. R., Feldman, D. R., & Risser, M. D. (2023). Future increases in North American extreme precipitation in CMIP6 downscaled with LOCA. *Journal of Hydrometeorology*, 24(5), 951–975. <https://doi.org/10.1175/JHM-D-22-0194.1>
- Pierce, D. W., Cayan, D. R., Goodrich, J., Das, T., & Munévar, A. (2022). Evaluating global climate models for hydrological studies of the upper Colorado River Basin. *JAWRA Journal of the American Water Resources Association*, 58(5), 709–734. <https://doi.org/10.1111/1752-1688.12974>
- Polade, S. D., Gershunov, A., Cayan, D. R., Dettinger, M. D., & Pierce, D. W. (2017). Precipitation in a warming world: Assessing projected hydro-climate changes in California and other Mediterranean climate regions. *Scientific Reports*, 7(1), 10783. <https://doi.org/10.1038/s41598-017-11285-y>
- Polade, S. D., Pierce, D. W., Cayan, D. R., Gershunov, A., & Dettinger, M. D. (2014). The key role of dry days in changing regional climate and precipitation regimes. *Scientific Reports*, 4(1), 4364. <https://doi.org/10.1038/srep04364>
- Rahimi, S. (2024). CMIP6 GCMs downscaled using WRF (Version 1) [Dataset]. Amazon Web Services. Retrieved from <https://registry.opendata.aws/wrf-cmip6>
- Rahimi, S., Huang, L., Norris, J., Hall, A., Goldenson, N., Krantz, W., et al. (2024). An overview of the Western United States dynamically downscaled dataset (WUS-D3). *Geoscientific Model Development*, 17(6), 2265–2286. <https://doi.org/10.5194/gmd-17-2265-2024>

- Ramanathan, V., Crutzen, P. J., Kiehl, J. T., & Rosenfeld, D. (2001). Aerosols, climate, and the hydrological cycle. *Science*, 294(5549), 2119–2124. <https://doi.org/10.1126/science.1064034>
- Rind, D., Goldberg, R., & Ruedy, R. (1989). Change in climate variability in the 21st century. *Climatic Change*, 14(1), 5–37. <https://doi.org/10.1007/BF00140173>
- Risser, M. D., Collins, W. D., Wehner, M. F., O'Brien, T. A., Huang, H., & Ullrich, P. A. (2024). Anthropogenic aerosols mask increases in US rainfall by greenhouse gases. *Nature Communications*, 15(1), 1318. <https://doi.org/10.1038/s41467-024-45504-8>
- Risser, M. D., Collins, W. D., Wehner, M. F., O'Brien, T. A., Paciorek, C. J., O'Brien, J. P., et al. (2023). A framework for detection and attribution of regional precipitation change: Application to the United States historical record. *Climate Dynamics*, 60(3), 705–741. <https://doi.org/10.1007/s00382-022-06321-1>
- Rodgers, K. B., Lee, S.-S., Rosenbloom, N., Timmermann, A., Danabasoglu, G., Deser, C., et al. (2021). Ubiquity of human-induced changes in climate variability. *Earth System Dynamics*, 12(4), 1393–1411. <https://doi.org/10.5194/esd-12-1393-2021>
- Samset, B. H., Myhre, G., Forster, P. M., Hodnebrog, Ø., Andrews, T., Faluvegi, G., et al. (2016). Fast and slow precipitation responses to individual climate forcings: A PDRMIP multimodel study. *Geophysical Research Letters*, 43(6), 2782–2791. <https://doi.org/10.1002/2016GL068064>
- Schmidt, D. F., & Grise, K. M. (2021). Drivers of twenty-first-century US winter precipitation trends in CMIP6 models: A storyline-based approach. *Journal of Climate*, 34(16), 6875–6889. <https://doi.org/10.1175/JCLI-D-21-0080.1>
- Seager, R., Cane, M., Henderson, N., Lee, D.-E., Abernathy, R., & Zhang, H. (2019). Strengthening tropical Pacific zonal sea surface temperature gradient consistent with greenhouse gases. *Nature Climate Change*, 9(7), 517–522. <https://doi.org/10.1038/s41558-019-0505-x>
- Sen, P. B. (1968). Estimates of the regression coefficient based on Kendall's Tau. *Journal of the American Statistical Association*, 63(324), 1379–1389. <https://doi.org/10.1080/01621459.1968.10480934>
- Shulgina, T., Gershunov, A., Hatchett, B. J., Guirguis, K., Subramanian, A. C., Margulis, S. A., et al. (2023). Observed and projected changes in snow accumulation and snowline in California's snowy mountains. *Climate Dynamics*, 61(9–10), 4809–4824. <https://doi.org/10.1007/s00382-023-06776-w>
- Simpson, I. R., McKinnon, K. A., Kennedy, D., Lawrence, D. M., Lehner, F., & Seager, R. (2023). Observed humidity trends in dry regions contradict climate models. *Proceedings of the National Academy of Sciences USA*, 121(1), e2302480120. <https://doi.org/10.1073/pnas.2302480120>
- Sun, Q., Zhang, X., Zwiers, F., Westra, S., & Alexander, L. V. (2021). A global, continental, and regional analysis of changes in extreme precipitation. *Journal of Climate*, 34(1), 243–258. <https://doi.org/10.1175/JCLI-D-19-0892.1>
- Sun, Y., Solomon, S., Dai, A., & Portmann, R. W. (2007). How often will it rain? *Journal of Climate*, 20(19), 4801–4818. <https://doi.org/10.1175/JCLI4263.1>
- Swain, D. L., Langenbrunner, B., Neelin, J. D., & Hall, A. (2018). Increasing precipitation volatility in twenty-first-century California. *Nature Climate Change*, 8(5), 427–433. <https://doi.org/10.1038/s41558-018-0140-y>
- Tao, W.-K., Chen, J.-P., Li, Z., Wang, C., & Zhang, C. (2012). Impact of aerosols on convective clouds and precipitation. *Reviews of Geophysics*, 50(2), RG2001. <https://doi.org/10.1029/2011RG000369>
- Tijerina, D. (2019). HUC8 – CONUS shapefile (version 1) [Dataset]. *Hydroshare*. Retrieved from <http://www.hydroshare.org/resource/b832a6c2f96541808444ec9562c5247e>
- Trenberth, K. E. (1999). Conceptual framework for changes of extremes of the hydrological cycle with climate change. In T. R. Karl, N. Nicholls, & A. Ghazi (Eds.), *Weather and climate extremes*. Springer. https://doi.org/10.1007/978-94-015-9265-9_18
- Tseng, K.-C., Johnson, N. C., Kapnick, S. B., Cooke, W., Delworth, T. L., Jia, L., et al. (2022). When will humanity notice its influence on atmospheric rivers? *Journal of Geophysical Research: Atmospheres*, 127(9), e2021JD036044. <https://doi.org/10.1029/2021JD036044>
- Varuolo-Clarke, A. M., Smerdon, J. E., Williams, A. P., & Seager, R. (2021). Gross discrepancies between observed and simulated twentieth-to-twenty-first-century precipitation trends in southeastern South America. *Journal of Climate*, 34(15), 6441–6457. <https://doi.org/10.1175/JCLI-D-20-0746.1>
- Vose, R. S., Applequist, S., Squires, M., Durre, I., Menne, M. J., Williams Jr, C. N., et al. (2014). NOAA monthly U.S. Climate gridded dataset (NClimGrid) (version 1). [Dataset]. *NOAA National Centers for Environmental Information*. <https://doi.org/10.7289/V5SX6B56>
- Vose, R. S., Applequist, S., Squires, M., Durre, I., Menne, M. J., Williams Jr, C. N., et al. (2014). Improved historical temperature and precipitation time series for US climate divisions. *Journal of Applied Meteorology and Climatology*, 53(5), 1232–1251. <https://doi.org/10.1175/JAMC-D-13-0248.1>
- Wilks, D. S. (1997). Resampling hypothesis tests for autocorrelated fields. *Journal of Climate*, 10(1), 65–82. [https://doi.org/10.1175/1520-0442\(1997\)10<0065:RHTFAF>2.0.CO;2](https://doi.org/10.1175/1520-0442(1997)10<0065:RHTFAF>2.0.CO;2)
- Wilks, D. S. (2016). “The stippling shows statistically significant grid points”: How research results are routinely overstated and overinterpreted, and what to do about it. *Bulletin of the American Meteorological Society*, 97(12), 2263–2273. <https://doi.org/10.1175/BAMS-D-15-00267.1>
- Williams, A. P. (2024). GHCN-daily: Western United States precipitation dataset (Version 1) [Dataset]. *Dryad*. <https://doi.org/10.5061/dryad.c866t1gfp>
- Williams, A. P., Cook, B. I., & Smerdon, J. E. (2022). Rapid intensification of the emerging southwestern North American megadrought in 2020–2021. *Nature Climate Change*, 12(3), 232–234. <https://doi.org/10.1038/s41558-022-01290-z>
- Wu, P., Christidis, N., & Stott, P. (2013). Anthropogenic impact on Earth's hydrological cycle. *Nature Climate Change*, 3(9), 807–810. <https://doi.org/10.1038/nclimate1932>
- Zhang, X., Alexander, L., Hegerl, G. C., Jones, P., Tank, A. K., Peterson, T. C., et al. (2011). Indices for monitoring changes in extremes based on daily temperature and precipitation data. *Wiley Interdisciplinary Reviews: Climate Change*, 2(6), 851–870. <https://doi.org/10.1002/wcc.147>